

Designing Potential Inhibitors Against RET PROTEIN TYROSINE KINASE DOMAIN to Fight Sporadic Medullary Thyroid Carcinoma: A Virtual Screening and Molecular Dynamics Simulation-Based Approach

Tanima Roy^a, Asif Abdullah^{b*}, Afiya Mubasharah^c, Ahmed Imtiaz Zamee^d, Md. Ibrahim Al Imran^{a*}, Md. Enamul Kabir Talukder^e, Md. Tofazzal Hosen^a, Dr. Muhammad Abdul Kadir^a, Muttakee Bin Ali^a

^aDepartment of Biomedical Physics and Technology, University of Dhaka, Dhaka 1000, Bangladesh

^bDepartment of Biomedical Engineering, Jashore University of Science and Technology, Jashore 7408, Bangladesh

^cDepartment of Biomedical Engineering, Bangladesh University of Engineering and Technology, Dhaka 1205, Bangladesh

^dDepartment of Information and Communication Technology, Bangladesh University of Engineering and Technology, Dhaka 1205, Bangladesh

^eDepartment of Genetic Engineering and Biotechnology, Jashore University of Science and Technology, Jashore 7408, Bangladesh

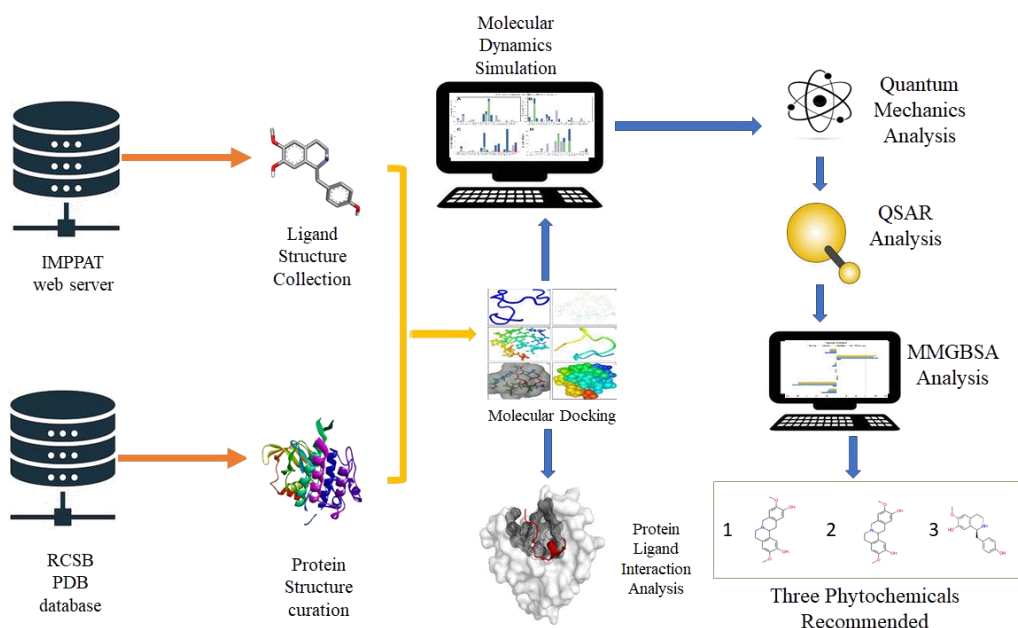
*Corresponding author, email: a.abdullah@just.edu.bd

*Corresponding author, email: imran.bmpt@du.ac.bd

ABSTRACT

Sporadic medullary thyroid cancer (sMTC) is a rare tumor originating in the thyroid's parafollicular cells, which secrete calcitonin. Structural complexity and a significant role in thyroid carcinoma cell growth make rearranged during transfection (RET) proto-oncogene a promising target for drug discovery. This work proposes the phytochemical screening of the soursop (*Annona muricata*) plant to uncover and unveil the yet unrecognized potential of phytochemicals from the soursop (*Annona muricata*) plant as effective inhibitors against RET proto-oncogene. via molecular docking studies, pharmacokinetic property analysis, quantitative structure-activity relationship (QSAR) analysis, molecular dynamic simulation, and quantum mechanics study. Among the compounds evaluated, IMPHY010968, IMPHY012644, and IMPHY001505 have demonstrated notably stronger binding affinities compared to the conventional drug Trametinib. Their respective docking scores, namely -8.6, -8.4, and -8.1, underline their promising potential. IMPHY0012644 exhibits the maximum molar refractivity at 95.05 and possesses the highest topological polar surface area (TPSA= 107.13 Å²) compared to other compounds. In the conducted studies, all other compounds fall within the standard range of $40 \leq MR$ (molar refractivity) ≤ 130 , and the TPSA value is noted for its stronger correlation with the system. In the case of the ligand compound IMPHY001505, the average Root Mean Square Deviation (RMSD) ranged from 1 to 3 Å, showcasing minimal fluctuations. Likewise, IMPHY010968 and IMPHY012644 demonstrated RMSD values within the 1-5 Å range. Conversely, the control drug CID_11707110 exhibited an elevated RMSD value ranging from 1 to 8 Å, indicating more significant oscillations when compared to our proposed compound. Selected compounds exhibit greater stability when compared to the control drug. Within the 175 to 185 residue index range, the control drug displays higher fluctuations than our proposed compounds. The Rg analysis indicates that IMPHY001505, IMPHY010968, and IMPHY012644 exhibit lower Rg values than the control drug over a 100 ns period, suggesting greater compactness. SASA values imply high exposure of amino acid residues in the complexes, indicating accessibility for further analysis. MolSA reveals standard van der Waals surface areas, while PSA highlights the compounds' polar interactions with the target protein. Overall, the selected compounds display favorable structural features for potential therapeutic applications.

Graphical Abstract



Graphical Abstract: Graphical workflow of the in-silico study. Phytochemicals were retrieved from the IMPPAT database, and target proteins were obtained from the RSCB PDB. After structure curation, molecular docking was performed followed by molecular dynamics simulation. Further analyses including quantum mechanics, QSAR, and MM/GBSA were carried out to assess binding stability and activity. Three top phytochemicals were identified for potential therapeutic use.

How to Cite: Tanima Roya, Asif Abdullah*, Afiya Mubasharahc, Ahmed Imtiaz Zameed, Md. Ibrahim Al Imrana*, Md. Enamul Kabir Talukdere, Md. Tofazzal Hosena, Dr. Muhammad Abdul Kadira, Muttakee Bin Alia, (2025) Designing Potential Inhibitors Against RET PROTEIN TYROSINE KINASE DOMAIN to Fight Sporadic Medullary Thyroid Carcinoma: A Virtual Screening and Molecular Dynamics Simulation-Based Approach, *Journal of Carcinogenesis*, Vol.24, No.3, 519-540.

1. INTRODUCTION

The RET receptor binds GDNF ligands. The glial cell line-derived neurotrophic factor family of ligands (GDNF) family includes four neurotrophic factors: GDNF, Neurturin (NRTN), artemin (ARTN), persephin (PSPN)(Ceccherini et al., 1993)(Knowles et al., 2006). The extracellular domain comprises cysteine-rich sites, calcium-binding sites, and four cadherin-like repeats (Airaksinen and Saarma, 2002) (Mani et al., 2001). The RET gene undergoes spontaneous alternative RNA splicing, producing three distinct isoforms of the RET protein, namely RET9, RET51, and RET43 (Myers et al., 1995). The RET gene is important in various biological processes, including spermatogenesis, the development of organs and tissues derived from the neural crest, cellular migration, signal transduction, and cell proliferation (Vargas-Leal et al., 2005). The RET gene can occasionally become an oncogene, leading to the development of various inherited and non-inherited illnesses. There are numerous methods for RET-RTK (receptor tyrosine kinase) to become oncogenic, including point mutations, chromosomal translocations, and genomic rearrangements. The human body develops many thyroid malignancies due to various RET proto-oncogene rearrangements. Neuroendocrine cells like parafollicular C-cells express receptor tyrosine kinase, encoded by RET (Wells Jr and Santoro, 2009). Blood calcium levels affect calcitonin secretion (Larsen and Kronenberg, 2011). The neural crest is the source of these parafollicular cells (Prete et al., 2020).

Medullary thyroid carcinoma (MTC) is believed to originate from parafollicular cells, also known as C cells. Papillary thyroid carcinoma, the most prevalent form of cancer, is frequently caused by the production of rearranged in-transformation/papillary thyroid carcinomas (RET/PTC) fusion proteins resulting from rearrangements within the RET gene. (Gautschi et al., 2017) (Yamaoka et al., 2018). Ultimately, oncogenic mutations and fusions in the RET proto-oncogene may transform RKTs into ligand-independent RKTs, a common situation in the thyroid (Terzyan et al., 2019).

RET inhibitors are widely used as drugs for sMTC. Numerous distinct tyrosine kinase inhibitors are currently identified, demonstrating anti-RET activity (Iams and Lovly, 2018). Several therapeutic interventions have been utilized in treating

individuals diagnosed with cancer linked to the RET gene and have demonstrated significant effectiveness in clinical environments. Several investigations have found genetic changes in the tyrosine kinase domain that cause RET kinase inhibitor resistance (Subbiah et al., 2018). Due to chemical structural differences, RET-tyrosine kinase inhibitors (RET-TKI) inhibit the RET kinase domain while the other resists it (Liu et al., 2018). Trametinib belongs to a class of drugs named kinase inhibitors. It restricts the abnormal protein's activity that signals the growth of cancer cells. Tyrosine kinase inhibitors target the active kinase domain to block intracellular tyrosine phosphorylation. This is because these tyrosine residues are often involved in cell proliferation (Huang et al., 2020)(Neves et al., 2018).

Utilization of virtual screening is widely employed in the field of drug discovery to identify novel compounds. Using in silico methods, primarily virtual screening, has become a valuable and cost-effective addition to in silico screening (Dey et al., 2023)(Hasan et al., 2022)(Morshed et al., 2022) for finding and developing new compounds that work well. Most of the time, ligand- and receptor-based virtual screening are used to search chemical databases for compounds projected to bind well to the target binding site (Banegas-Luna et al., 2018)(Kaushik et al., 2018). The 3D structure of the protein/ligand complex plays a vital role in molecular modeling and drug discovery (Stanzione et al., 2021)(Baral et al., 2022)(Bibi et al., 2022). QSAR, pharmacophore analysis, and biological tests can improve and produce innovative leads (Dipta et al., 2021)(Khan et al., 2021)(Munshi et al., 2022). Structure-based drug design plays a governing role in drug discovery by facilitating the creation of more potent and biologically relevant molecules (Abdullah et al., 2023)(Bhole et al., 2021)(Maurya et al., 2020). Molecular dynamics simulations, based on a comprehensive physicochemical model governing interatomic interactions, can forecast the motion of individual molecules within a molecular system (Feng et al., 2019)(Atofarati, n.d.)(Rahman et al., 2021).

The fundamental concept underlying molecular dynamics (MD) simulation is relatively simple. Given the presence of coordinates assigned to individual atoms within a biomolecular system, it becomes possible to approximate the magnitude of the forces experienced by each atom. This estimate considers the combined influence of all the system's atoms, such as those that comprise a protein enclosing a lipid bilayer and a water component (Sarker et al., 2022)(Islam et al., 2022). Predicting atoms' spatial positions over time is conceivable using Newton's equations of motion. One potential approach involves traversing temporal dimensions. The forces that are acting on each atom can be approximated, which makes it possible to modify the location and velocity of each atom in reaction to these forces. The subsequent step involves a comparative analysis between a three-dimensional representation of the system's configuration at each specific moment throughout the simulated duration and the resultant trajectory (Durrant and Mccammon, 2011)(Gkeka et al., 2020).

One of the most common drug development objectives is identifying a ligand to deliver a particular signaling profile and bind to the target. This is especially true for signaling receptors (Al Saber et al., 2022)(Biswas et al., 2022). Pharmacokinetic assays are an essential part of a new drug development program. These compounds assist in assessing the chronological sequence of drug administration and the detection of significant metabolites in different physiological fluids, thus enabling the investigation of drug uptake, distribution, metabolism, and elimination. Preclinical studies frequently utilize preclinical pharmacokinetic assays (PK) to evaluate toxicological outcomes. Pharmacokinetic-guided dose escalation (PGDE) methods aid in translating preclinical pharmacokinetic data into the clinical realm for therapeutic discovery during phase I investigations (Durrant and McCammon, 2011)(Hossain et al., 2023)(Dror et al., 2011).

PK studies for escalation and clinical trials for cures are critical. Absorption, distribution, metabolism, toxin (ADMET) studies and excretion must be considered during medication development and discovery. Effective composites with higher ADMET properties are crucial (Huang et al., 2015)(Arefin et al., 2021)(Biswas et al., 2021) (Jia et al., 2020). When developing new medicines, it is important to keep drug-likeness in mind from the beginning of the process. Lipinsky and colleagues proposed the first rule-based drug filter in 1997. It is advised that the molecular weight (MW) be less than 500, that the number of hydrogen bond acceptors (HBAs) be higher than or equal to 5, and that the water/octanol partition coefficient (Log P) be less than 5. The molecular weight (MW) should be less than 500, and the number of hydrogen bond acceptors (HBAs) and number of hydrogen bond donors (HBDs) should also be considered (Ferreira and Andricopulo, 2019)(Zhou et al., 2020)(Chen et al., 2020)(Chagas et al., 2018). In their study, Ghose and colleagues discovered that a significant majority (over 80%) of the 6,304 compounds included in their CMC database satisfied the specified criteria, namely: a logarithm of the octanol-water partition coefficient (log P) equal to -0.4, a molecular weight (MW) of 480 or less, a molar refractivity (MR) of 40, and a total atom count ranging from 20 to 70 (MahmutGür EdaAltınöz, NesrinŞener, ÇiğdemŞahin, MerveŞenturan, İzzetŞener, MuhammetÇavuş, Ergin MuratAltuner, 2023)(Olubode et al., 2022)(Glassman and Muzykantov, 2019). Studies reported that *Annona muricata* may be effective in treating thyroid carcinoma, but the probable effective compounds responsible for and can be used as an alternative drug against thyroid carcinoma are still unknown. This work thus focuses on the Phytochemical Screening of ligands derived from *Annona muricata* targeting to find novel compounds to fight thyroid carcinoma.

2. MATERIALS AND METHODS

Protein Preparation

The 3D structure of RET tyrosine kinase (PDB ID: 6NE7) from the RCSB Protein Data Bank was obtained from the RCSB PDB database. Employing Discovery Studio Visualizer and UCSF Chimera software, tasks were executed with specific purposes: removal of metal ions and water for structural clarity, elimination of cofactors to isolate the protein, insertion of polar hydrogen particles to enhance solubility, integration of nonpolar hydrogen particles for hydrophobic interactions, and determination of Gasteiger charges using AutoDock Tools for subsequent molecular docking analyses (Mahato and Sidorova, 2020).

Selection of Ligands

IMPPAT database has been used for an advanced screening of the phytochemicals of the *Annona muricata* plant (Soursop) (Mohanraj et al., 2018). Totaling 234 structures in SDF file format were downloaded from the database, and undergo essential pre-processing steps. the ligands are subjected to energy minimization using the UFF force field and a conjugate gradients optimization algorithm within PyRx software. This involves iteratively adjusting the ligand conformations to achieve stable energy states. A total of 2000 optimization steps are executed to ensure thorough refinement. Subsequently, protonation states are adjusted to mimic physiological conditions, ensuring accuracy in binding predictions for effective docking studies, and enhancing the reliability and precision of the subsequent molecular docking analyses.

Molecular Docking

Molecular docking was conducted using PyRx software to assess the interaction between the target protein and a compound (Ko et al., 2005). The active site of the protein served as the designated pocket for docking simulations, enabling a thorough exploration of potential binding modes. The results were then exported in CSV format for systematic analysis. Subsequently, the compound with the highest binding energy was cross-validated 3 times and selected for further investigation into protein-ligand interactions. (Dallakyan and Olson, 2015).

Pharmacokinetic Property

Understanding the dynamic movement of drugs into and out of the body over time is crucial, as it correlates with both the duration and intensity of these processes (Hsiao et al., 2021). At the beginning of CADD, understanding pharmacokinetics is essential for determining the effectiveness and durability of compounds. Utilizing the SwissADME server, this study assessed the preliminary pharmacokinetic properties of the phytochemicals (Briggs et al., 2002). Utilizing the PKCSM server, the toxicity profile was predicted.

Molecular Mechanics with Generalised Born and Surface Area Solvation (MM-GBSA) and Quantum Mechanics Analysis

Examining a ligand's conformation within a protein's binding site is crucial in determining potential active conformations, binding affinities, and associated strains during the binding event. structural optimizations and minimum energy conformations need to be figured out to reach this type of binding event, which relies on how much energy is in the solution phase and how much is in the gas phase. There is a requirement for improvements to the conventional molecular mechanics (MM) approach to represent a ligand-protein complex system incorporating metal ions accurately. The ligand minimization procedure entailed the application of quantum mechanical computations employing the Density Functional Theory (DFT) as implemented in the Jaguar v-10.962 software. The B3LYP method, which uses the Becke exchange function and the Lee, Yang, and Parrs (LYP) correlation function, was used to figure out the DFT. The calculations were performed using the 6-31G(d,p) basis set. As a result, after identifying the docking score with the highest value and applying MM-GBSA, the ligand was selected for additional examination utilizing either DFT or QM calculations (Pearson, 1986). The energy gap between the compounds' highest occupied molecular orbitals (HOMOs) and lowest unoccupied molecular orbitals (LUMOs) was predicted by DFT calculations. To assess the relative hardness and softness of the pharmaceutical substances, an analysis was conducted on the frontier molecular orbital energies (ϵ) of both the HOMOs and LUMOs. The analysis used the Koopmans theorem equation (Equation 2) and the interpretive equation that Parr and Pearson proposed (Equation 1). The hardness value provides insight into the atom's resistance to charge transfer to another atom or metal surface, whereas the softness value aids in assessing the atom's electron-receiving capacity. (Cao et al., 2019) (Genheden et al., 2012). The following Equations can be used to measure the chemical hardness (1) and softness (2).

$$\text{Hardness}, (\eta) = \frac{(1 - A)}{2} \dots \dots (1)$$

$$\text{Softness}, (S) = \frac{1}{\eta} \dots \dots (2)$$

Molecular Dynamic Simulation

To achieve the desired level of protein stability, the RET receptor's interaction with the three feasible ligand molecules was initially selected and then put through one hundred nanoseconds of MD simulations. To mannequin, the molecular dynamics of the protein-ligand complicated constructions, “Desmond v3.6 Program” (paid version) from Schrodinger (<https://www.schrodinger.com/ac>) was employed (Omar et al., 2023). A predetermined water approach named TIP3P was formerly developed to build the privileged frame to organize a precise volume with periodic orthorhombic equals separated using 10 mm. In this water approach, 3 points rigid water patch with charges as well as parameters of Lennard- Jones is attributed to each of the three patches of the targeted protein.

To neutralize the framework electrically, the essential ions, for example, 0+ and 0.15M salts, have been randomly brought to the solvent. The solvency protein machine used to be built utilizing a ligand complex, and the device framework once decreased the default protocol's usage. This was done interior the Desmond module using the pressure subject settings OPLS3e (Ahammad et al., 2021). At 101,325 bar (1 atm) strain, NPT assemblies have been sustained, and it also needs 300 K with 50 PS for capturing sessions and a total of 1.2 kcal/mole electricity entering earlier than them, the isotropic process and temperature mixture of Nose–Hoover has been employed. The molecular dynamic simulation screen captures have been prompted by the utility of Schrodinger’s maestro application, version 9.5. The Simulations interplay layout derived from the Desmond modules of the Schrodinger batch has been used to dissect the simulation match and examine the MD simulation dependability.

Here, root means square deviation (RMSD), trajectory performance, root mean square fluctuation (RMSF), solvent-accessible surface area (SASA) value, the radius of gyration (Rg) value, intramolecular hydrogen bonds, protein-ligand contacts (PL), MolSA and the polar surface area (PSA) evaluate the protein-ligand complicated shape balance.

Ligand Activity Prediction by QSAR Analysis

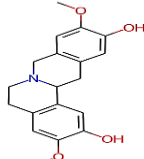
The evaluation of the relative effectiveness of the three identified phytochemicals and the control drug was conducted utilizing the PASS (Prediction of Activity Spectra for Substances) server, a well-established resource accessible at <http://www.way2drug.com/passonline/>. The server utilizes the structural characteristics of a substance to predict its potential outcomes. (Ban et al., 2018). The investigation into the likelihood of a particular substance being categorized in both the active and inactive subsets of that substance was carried out using the Structure-Activity Relationship Base (SAR Base). The molecular structure of the phytochemicals was depicted using the SMILES (Simplified Molecular Input Line Entry System) format. Afterward, the Pa (probable activity) and Pi (probable inactivity) values were calculated for each ligand (Roos et al., 2019).

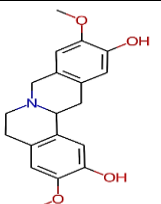
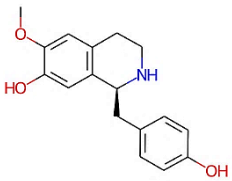
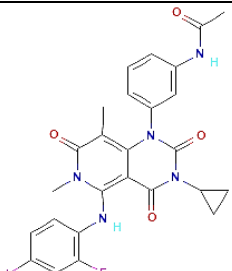
3. RESULTS

Molecular Docking Result Analysis

The IMPPAT database hits 234 phytochemicals of the *Annona muricata* plant, of which ten phytochemicals are from bark, 92 phytochemicals are from fruit, 118 phytochemicals are from leaf, seven phytochemicals are from seed, seven phytochemicals are from the root. The minimum docking score is -3.5 kcal/mol, and the maximum docking score is -10.5 Kcal/mol. Ligands with higher docking results that doesn’t satisfy any of the Lipinski, Ghose, Veber, Egan, and Muegge rules are excluded from the study. The highest docking result for a compound is -8.6 Kcal/mol considering the compounds that don’t violate any of the following. This study used trametinib as a control ligand due to its previously reported inhibitory effect on cancer cell growth, associated with a binding score of -7.9 kcal/mol. The compounds with the best docking score and binding affinities are listed in **Table 1**.

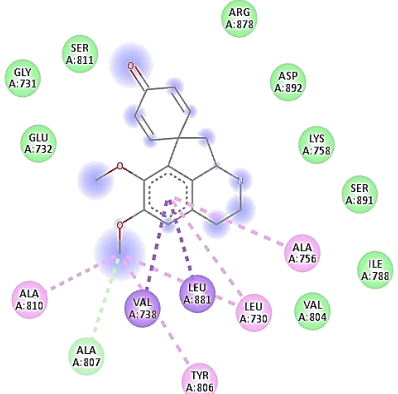
Table 1: Chemical name, PubChem CID, two-dimensional (2D) chemical structure, and docking score for the top three ligands and Trametinib (control)/

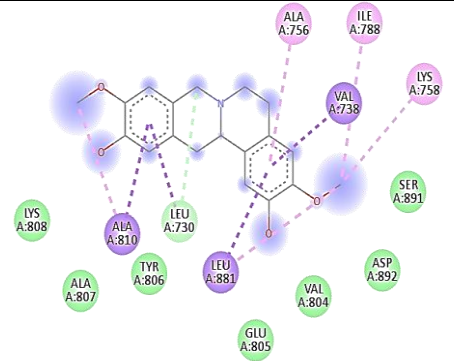
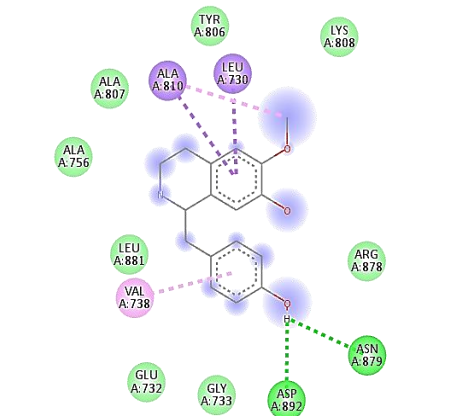
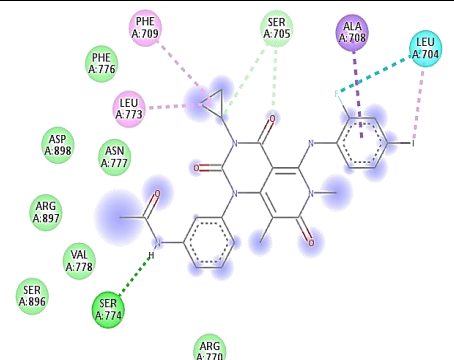
Compound CID	Compound Name	Compound Structure	Dockin g Score (Kcal/ mol)
IMPHY010968	(4S)-10,11-dimethoxyspiro[5-azatricyclo[6.3.1.0 ⁴ ,12]dodeca-1(12),8,10-triene-2,4'-cyclohexa-2,5-diene]-1'-one		-8.6

IMPHY012644	(-)-Coreximine		-8.4
IMPHY001505	Coclaurine		-8.1
CID 11707110	Trametinib (control)		-7.9

The interactions that occur between proteins and ligand molecules play a crucial role in a wide range of biological procedures. Chemical bonding plays a pivotal role in facilitating these interactions, as the concept of molecular complementarity enables it. Cellular processes are accurately regulated by ligand-target protein interactions. These interactions serve as the basis for coordinating vital processes within biological cells. **Table 2** depicts the protein-ligand interaction of the selected compounds concerning the control drug.

Table 2: Protein-ligand interaction between different ligands and the target protein. In the interaction diagram, the conventional hydrogen bonds are marked with shamrock green; Van Der Waals bonds with olive green, Carbon hydrogen bonds with emerald green, and Pi sigma bonds with violet color

Compound CID	Protein-Ligand Interaction Diagram	Conventional Hydrogen Bonds	Van Der Waals bonds	Carbon-Hydrogen bonds	Pi-Sigma bonds
IMPHY01096 8		-----	ARG(A:878), SER(A:811), GLY(A:731), GLU(A:732), GLU(A:806), ASP(A:892), SER(A:891), LYS(A:758), VAL(A:804), GLU(A:805) and ALA(A:807)	LEU(A:730)	LEU(A:881)

IMPHY01264 4		-----	LYS(A:728), LYS(A:808), ALA(A:808), TYR(A:807), GLU(A:806), VAL(A:805), ILE(A:804), SER(A:788) and ASP(A:891)	LEU(A:730) and ASP(A:892)	ALA(A:810), LEU(A:881) and VAL(A:738)
IMPHY00150 5		ASP A:892 and ASN A:879	GLY(A:733), GLU(A:732), LEU(A:881), ALA(A:756), ALA(A:807), TYR(A:806) and LYS(A:808)	-----	ALA(A:810) and ASN(A:879)
CID 11707110		SER(A:774)	SER(A:705), PHE(A:776), ASN(A:777), ASP(A:898), LEU(A:870), ARG(A:897), VAL(A:778), SER(A:896) and ARG(A:770)	-----	LEU(A:773) and PHE(A:709)

The interaction network between various ligands and the target protein is depicted, showcasing distinct protein-ligand interactions. In the illustrative diagram, conventional hydrogen bonds are color-coded in shamrock green, Van Der Waals bonds in olive green, Carbon hydrogen bonds in emerald green, and Pi sigma bonds in violet. IMPHY010968 exhibits an absence of conventional Hydrogen Bonds but forms Van der Waals bonds with strategic residues like ARG(A:878), SER(A:811), GLY(A:731), GLU(A:732), GLU(A:806), ASP(A:892), SER(A:891), LYS(A:758), VAL(A:804), GLU(A:805), and ALA(A:807). Additionally, carbon-hydrogen bonding is observed with LEU(A:730), and a pi-sigma bond forms with LEU(A:881), Alkyl and Pi-alkyl bonds formed with ALA (A:756), TYR (A:806) VAL (A:738), ALA (A:810) [designated with mild pink in **Table 2**]. The protein-ligand interaction profile for IMPHY012644 reveals a distinctive pattern. Notably, there are no conventional hydrogen bonds formed. Instead, Van der Waals bonds are established with strategic residues, including LYS(A:808), ALA(A:808), TYR(A:807), GLU(A:806), VAL(A:805), ILE(A:804), SER(A:788), and ASP(A:891). Furthermore, Carbon Hydrogen bonds manifest with LEU(A:730) and ASP(A:892), while pi sigma bonds are observed with ALA(A:810), LEU(A:881), and VAL(A:738). Alkyl and pi-alkyl bonds contribute to the interaction profile, notably with LYS (A:758) and ALA (A:756). IMPHY001505's interaction with the target protein is characterized by specific bond formations. Notably, conventional hydrogen bonds are established with ASP(A:892) and ASN(A:879). Van der Waals bonds are formed with GLY(A:733), GLU(A:732), LEU(A:881), ALA(A:756), ALA(A:807), TYR(A:806), and LYS(A:808). Interestingly, no carbon-hydrogen bonds are observed. Pi sigma bonds occur with ALA(A:810) and ASN(A:879), while Alkyl and Pi alkyl bonds are established with VAL(A:738). The control drug CID_11707110 exhibits a diverse array of interactions with the target protein. Conventional hydrogen bonds are formed with SER(A:774), while van der Waals bonds strategically involve SER(A:705), PHE(A:776), ASN(A:777), ASP(A:898), LEU(A:870), ARG(A:897), VAL(A:778), SER(A:896), and ARG(A:770). No carbon-

hydrogen bonds are observed. However, pi-sigma bonds are formed with LEU(A:773) and PHE(A:709), and Alkyl and Pi-alkyl bonds are established with LEU(A:773) and PHE(A:709). A noteworthy interaction involves a fluorine halogen bond with LEU(A:704) [Marked as cyan in **Table 2**]. This comprehensive interaction profile delineates the complex binding dynamics of the phytochemicals and the control drug with the target protein.

Pharmacokinetic Property Analysis

The basic physiochemical properties of the selected drug compound have been depicted in **Table 3**. All the selected ligands follow Lipinski, Ghose, Veber, Egan, and Muegge rules, as violating these rules results in problems with bioavailability. IMPHY0012644 has the highest molar refractivity (95.05) and topological polar surface area (TPSA= 107.13 Å²) among the compounds. All the other compounds have obtained a standard value of $40 \leq MR$ (molar refractivity) ≤ 130 in the studies, and the TPSA value refers to the higher correlation with the system.

Table 3: Physiochemical Properties of the selected compounds

Compound ID	Molecular weight (g/mol)	Num. heavy atoms	Num. arom. heavy atoms	Fraction Csp ³	Num. rotatable bonds	Num. H-bond acceptors	Num. H-bond donors	Molar Refractivity	TPSA (Å ²)
IMPHY010968	297.35	22	6	0.39	2	4	1	87.48	47.56
IMPHY012644	327.37	24	12	0.37	2	5	2	95.05	62.16
IMPHY001505	285.34	21	12	0.29	3	4	3	85.62	61.72
CID 11707110 (Control)	615.39	37	22	0.23	6	5	2	149.59	107.13

The basic pharmacokinetic properties are very important to figure out the drug-likeness of the molecules. **Table 4** represents some of the major pharmacokinetic properties of the selected ligands, including intestinal absorption, Blood-brain barrier (BBB) permeability, inhibitory information, and skin permeation.

Table 4: Pharmacokinetic Properties of the selected ligands

Compound ID	Intestinal Absorption	BBB permeant (log BB)	P-gp substrate	CYP1A2 inhibitor	CYP2C19 inhibitor	CYP2C9 inhibitor	CYP2D6 inhibitor	CYP3A4 inhibitor	Log Kp (skin permeation) (cm/s)
IMPHY010968	94.57%	0.084	Yes	Yes	No	Yes	No	Yes	-6.64
IMPHY012644	91.76%	0.199	Yes	No	No	No	Yes	No	-6.46
IMPHY001505	94.14%	0.029	Yes	No	No	No	Yes	No	-6.21
CID 11707110 (Control)	89.72%	-0.765	No	No	Yes	Yes	No	Yes	-7.62

All the recommended ligands have a high intestinal absorption ratio compared to the control drug and belong to the p-glycoprotein substrate. IMPHY010968 works as CYP1A2, CYP2C9, CYP3A4 inhibitor, whereas IMPHY012644 and IMPHY001505 function as CYP2D6 inhibitor.

Table 5: Toxicity Table of the selected phytochemicals

Compound ID	AMES Toxicity	Max. tolerated dose (human) (log mg/kg/day)	hERG I inhibitor	hERG II inhibitor	Oral Rat Acute Toxicity (LD50) (mol/kg)	Oral Rat Chronic Toxicity (LOAEL) (log mg/kg_bw/day)	Hepatotoxicity	Skin Sensitisation	T.Pyiformis toxicity (log ug/L)	Minnow toxicity (log mM)
IMPHY001505	No	-0.347	No	Yes	2.634	1.019	No	No	0.527	0.627
IMPHY010968	Yes	0.44	No	No	2.482	3.366	No	No	0.285	5.512
IMPHY012644	No	-0.449	No	Yes	2.859	1.259	No	No	0.486	0.562
CID-11707110 (control)	No	0.319	No	Yes	3.097	0.18	Yes	No	0.285	0.928

From the toxicity **Table 5**, it can be visualized that only IMPHY 010968 showed AMES toxicity. IMPHY001505 and IMPHY012644 can inhibit hERG II. Understanding the acute oral toxicity of medicine in rats is essential for drug risk management. This toxicity is frequently quantified using the 50% lethal dose (LD50), which refers to the quantity of the chemical anticipated to result in the death of fifty percent of the animals treated over a set amount of time. The phytochemicals we prescribe have a lower oral rat acute toxicity compared to the medicine used as a control, trametinib. The chemical IMPHY010968 has AMES toxicity. The phytochemicals recommended won't cause skin sensitization. In contrast to the hepatotoxicity seen by trametinib, the phytochemicals proposed are predicted to have no hepatotoxic effects in the in-silico study.

MD Simulation

In computer-aided drug development, MD simulation is executed to perceive a real-time protein-ligand architecture's intermolecular interaction and strength. The method can also predict changes in the shape of a complex system that was revealed to an artificial in nature. To better understand the alterations to the protein complex's architecture, a 100 ns MD simulation of the specific ligand-coupled protein was performed in this study. The intermolecular nature was initially analyzed by using the last 100 ns of MDS trajectories as snapshots.

RMSD Analysis

The mean change in this protein-ligand interaction's root-mean-square deviation (RMSD) is deemed acceptable, with a range of approximately 1–4 Å. Values exceeding this range indicate a significant variance in the configuration of the protein complex. To examine how such structural changes will affect the selected protein when combined with three ligands Coclaurine [IMPHY001505], (-)-Coreximine [IMPHY012644] and (4S)-10,11-dimethoxyspiro[5-azatricyclo[6.3.1.0^{4,12}]dodeca-1(12),8,10=triene-2,4'-cyclohexa-2,5-diene]-1'-one [IMPHY010968]), a 100 ns molecular dynamics simulation was performed, and the RMSD value was computed.

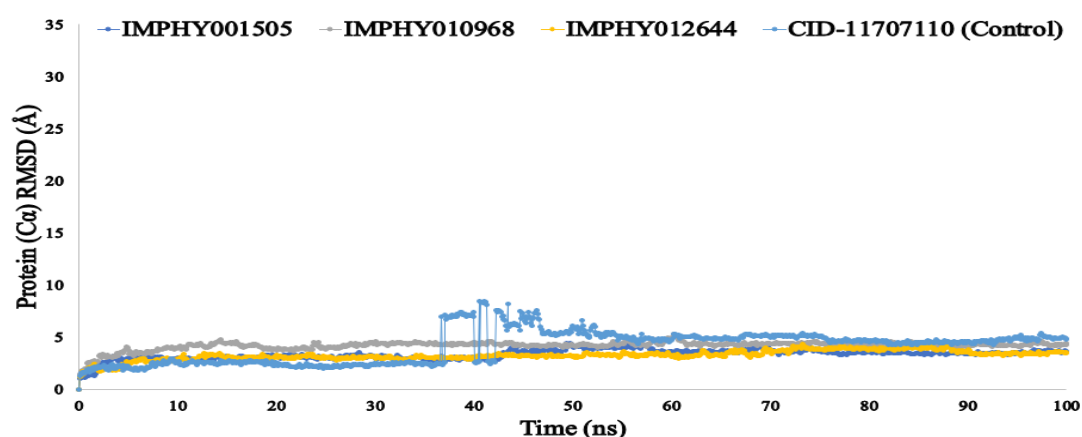


Figure 1: Root Mean Square Deviation (RMSD) values for the 6NE7 protein model, showcasing its interaction with three ligand compounds (IMPHY001505, IMPHY010968, and IMPHY012644) and a control drug CID 11707110. The RMSD values are derived from the Ca atoms of the complex system. The compounds IMPHY001505, IMPHY010968, and IMPHY012644 are visually distinguished by deep blue, ash, and yellow colors, respectively, while the control drug is depicted in blue.

When considering ligand compound interactions with the 6NE7 protein model, a detailed analysis of RMSD values uncovers specific patterns. The ligand compound IMPHY001505 showed an average RMSD of 1-3 Å, indicating minimal fluctuations. Similarly, IMPHY010968 and IMPHY012644 showed RMSD values ranging from 1 to 5 Å, suggesting stable interactions. On the other hand, the control drug CID_11707110 showed a higher RMSD value, varying between 1-8 Å. The heightened variability indicates more fluctuations when compared to our suggested compound. As shown in **Figure 1**, there was minimal variation within an appropriate range, highlighting the structural stability of the protein-ligand complex. Highlighting the benefits of our suggested compound in establishing a stable interaction with the protein model.

RMSF Analysis

The RMSF can help signify the local modifications within the protein chain when certain ligand compounds bind with particular residues. Thus, the RMSF values of IMPHY001505, IMPHY010968, IMPHY012644, and a control drug with a designated protein model were determined to examine the changes in protein structural flexibility brought on by attaching certain ligand compounds to a particular residue position, as shown in **Figure 2**.

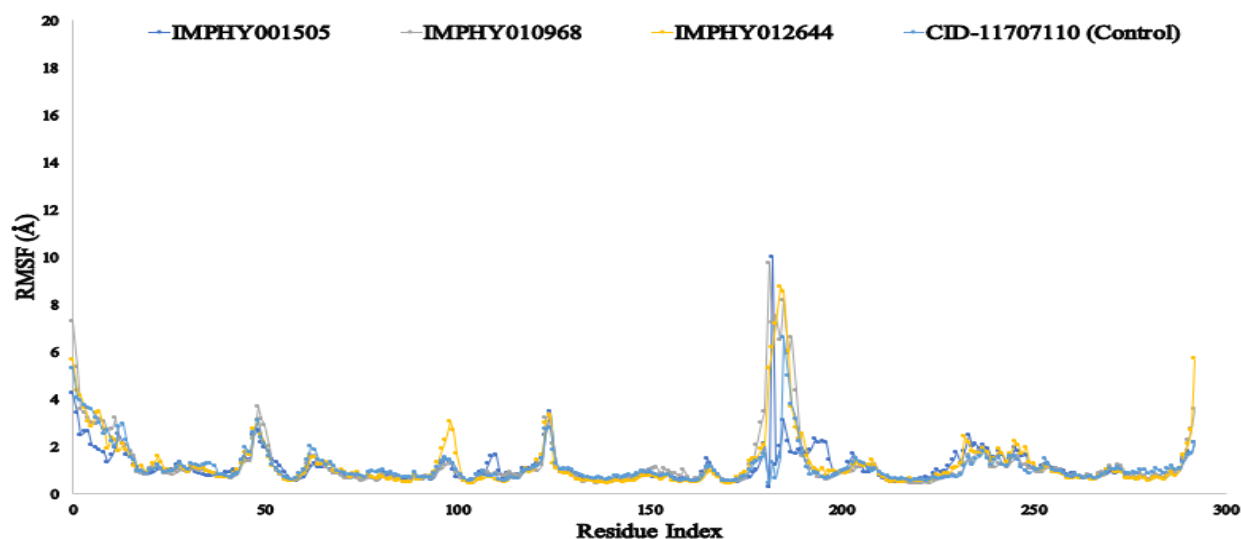


Figure 2: Visualization of Root Mean Square Fluctuation (RMSF) values derived from the Ca atoms of a 6NE7 protein model complex system, incorporating interactions with three ligand compounds and a control drug. The compounds IMPHY001505, IMPHY010968, and IMPHY012644 are distinguished by deep blue, ash, and yellow hues, respectively, with the control drug represented in blue. The color-coded representation aids in the identification and comparison of the fluctuation patterns

Exploring the secondary structural components, such as alpha-helices and beta-strands, revealed a significant frequency distribution ranging from 5 to 170 amino acid residues with minimal fluctuation. The heightened fluctuations were primarily observed at the protein's extremities due to the presence of N- and C-terminal domains. It suggests that in the simulated setting, the chances of minimal variation in the movement of an individual atom are consistent across all three ligand compounds studied. Our finalized compounds, in particular, showed improved stability in comparison to the control drug. It is worth mentioning that the control drug showed increased fluctuations, particularly in the 175 to 185 residue index range, emphasizing the superior stability of our proposed compounds. Quantifying these observations involved calculating the median Root Mean Square Fluctuation (RMSF) values for IMPHY001505, IMPHY010968, IMPHY012644, and the control drug CID-11707110, which were 0.892 Å, 0.874 Å, 0.894 Å, and 0.932 Å, respectively. This thorough examination highlights the enhanced stability and decreased fluctuations demonstrated by our suggested ligand compounds when compared to the control drug.

Rg Analysis

The Radius of Gyration (Rg) of a protein-ligand interaction system is described by the arrangement of its atoms along its axis. Evaluation of Rg is a key signal when attempting to anticipate the structural functioning of a macromolecule since it reflects changes in the compactness of the complex over time. The arrangement of an interaction system's atoms along its axis can provide information on the Radius of Gyration (Rg) of a protein-ligand complex. When trying to anticipate the structural functioning of a macromolecule, the evaluation of Rg is a critical signal since it indicates changes in the compactness of the complex over time. These changes can be seen as a result of many processes.

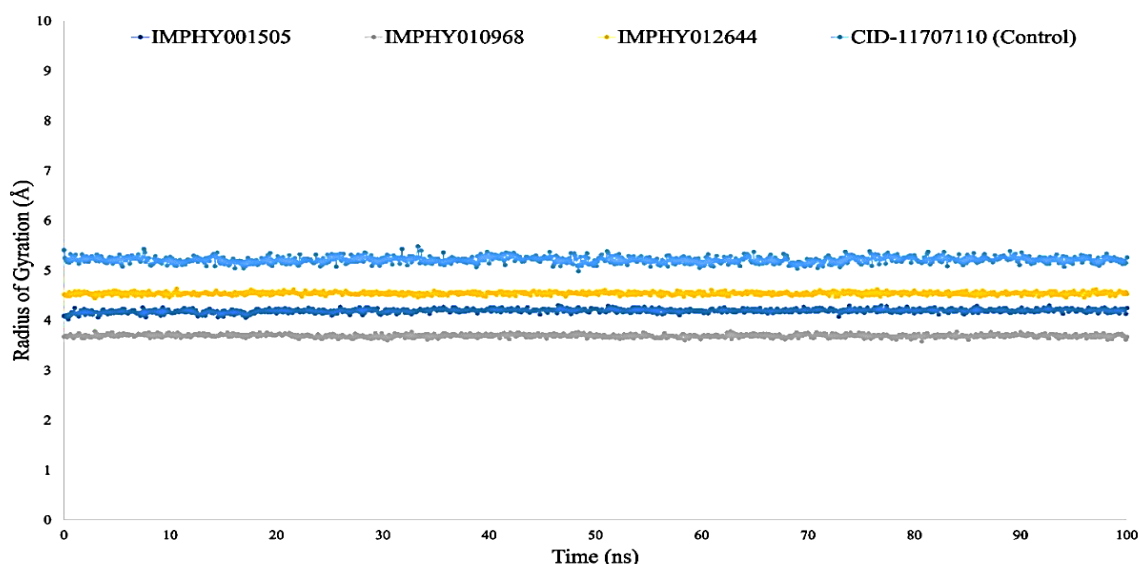


Figure 3: Radius of gyration (Rg) values over a 100 ns time frame, encompassing engagements with three ligand compounds and a control drug, the compounds IMPHY001505, IMPHY010968, and IMPHY012644 are delineated by deep blue, ash, and yellow tones, respectively, while the control drug is depicted in blue.

This study conducted a thorough analysis of compound stability within the target protein context by examining Radius of Gyration (Rg) values over a 100 ns time frame, as shown in **Figure 3**. Notably, the average Rg values for each compound were determined as follows: 4.0 (IMPHY001505), 3.8 (IMPHY010968), 4.5 (IMPHY012644), and 5.5 (control drug). The Rg parameter is used to gauge the compactness of a protein-ligand complex, where higher values suggest decreased compactness. During our study, the chosen compounds showed significantly reduced Rg values in comparison to the control drug. It indicates a more condensed and steady structure for the protein-ligand complexes created with our suggested compounds. The decrease in Rg values for IMPHY001505, IMPHY010968, and IMPHY012644 highlights their strong capability to form a more stable interaction with the target protein.

Analysis of SASA, MolSA and PSA

SASA controls biological macromolecule structure and function. In most situations, amino acid residues on a protein's surface operate as active sites or interact with other molecules and ligands, which helps us understand the molecule's hydrophilic or hydrophobic nature and protein-ligand interaction components.

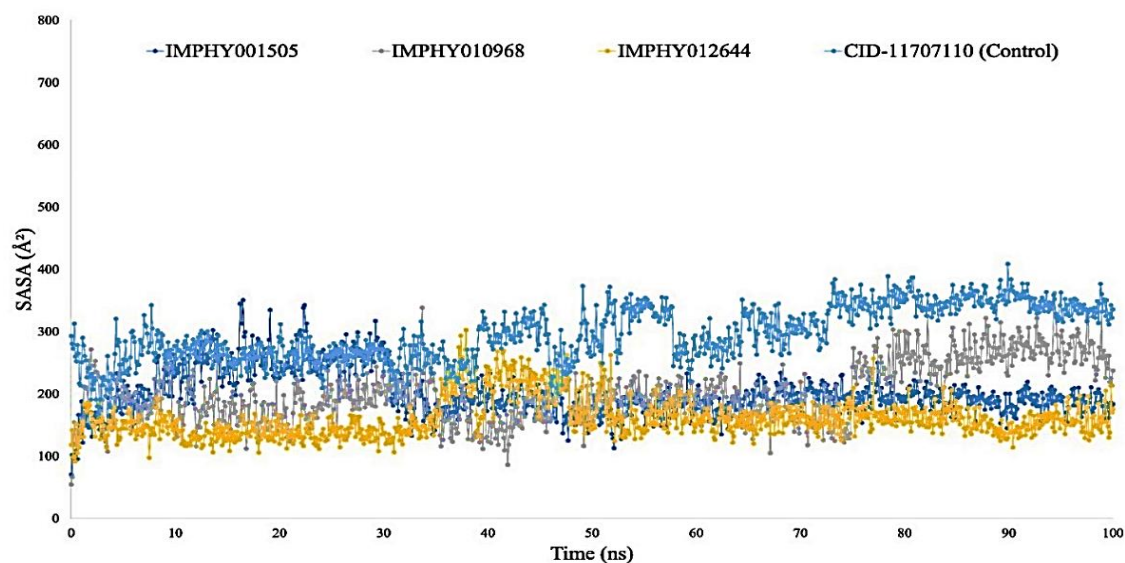


Figure 4: The solvent accessible surface area (SASA) of the protein-ligand interaction compounds was calculated from the 100 ns simulation interaction diagram. Deep Blue, ash, yellow and blue colors were employed to represent IMPHY001505, IMPHY010968, IMPHY012644, and the control drug, respectively

The SASA value of the protein complexed with the four ligand compounds IMPHY001505, IMPHY010968, IMPHY012644, and the control drug was determined and plotted in **Figure 4**. The average SASA value ranged from 50 to 320 Å², indicating a high level of exposure of amino acid residues to the chosen compound in the given system. As a result, these findings demonstrate that such complexes are highly exposed and likely accessible for further analysis.

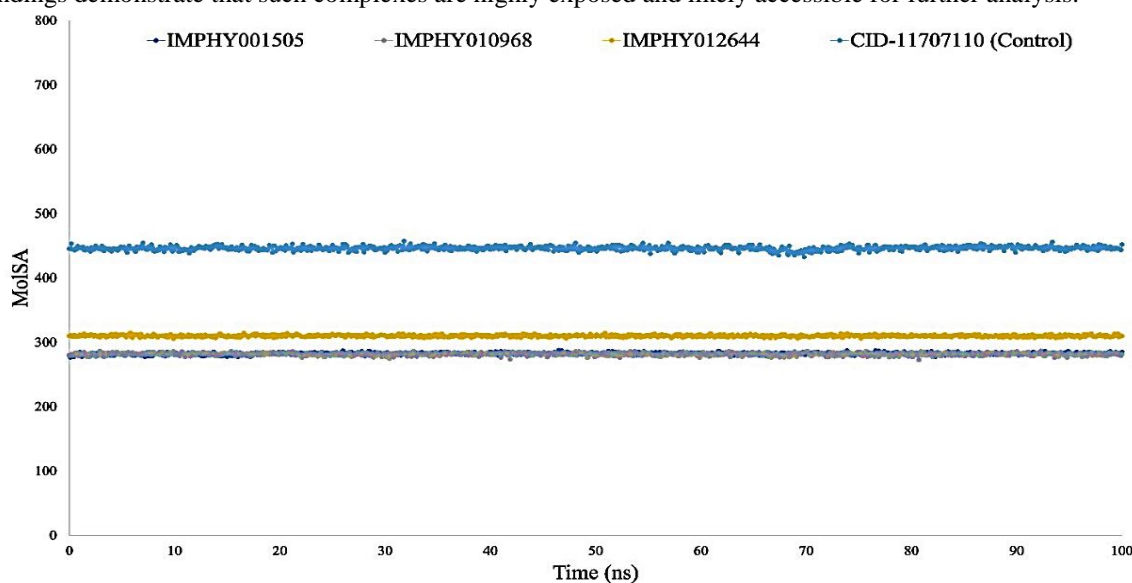


Figure 5: The MolSA of the protein-ligand interaction compounds was calculated from a 100 ns simulation diagram, and IMPHY001505, IMPHY010968, IMPHY012644, and control drug were represented by Deep blue, ash, yellow, and blue colors, respectively

The Molecular Surface Area (MolSA) is equivalent to a van der Waals surface area which can be calculated using a 1.4 Å probe radius. In our in-silico study, IMPHY001505, IMPHY010968, IMPHY012644, and the control drug had the standard van der Waals surface area (**Figure 5**). Additionally, a molecule's Polarity Surface Area (PSA) is mainly contributed by oxygen and nitrogen atoms. IMPHY001505, IMPHY010968, IMPHY012644, and the control drug showed high PSA values when interacting with the target protein (**Figure 6**).

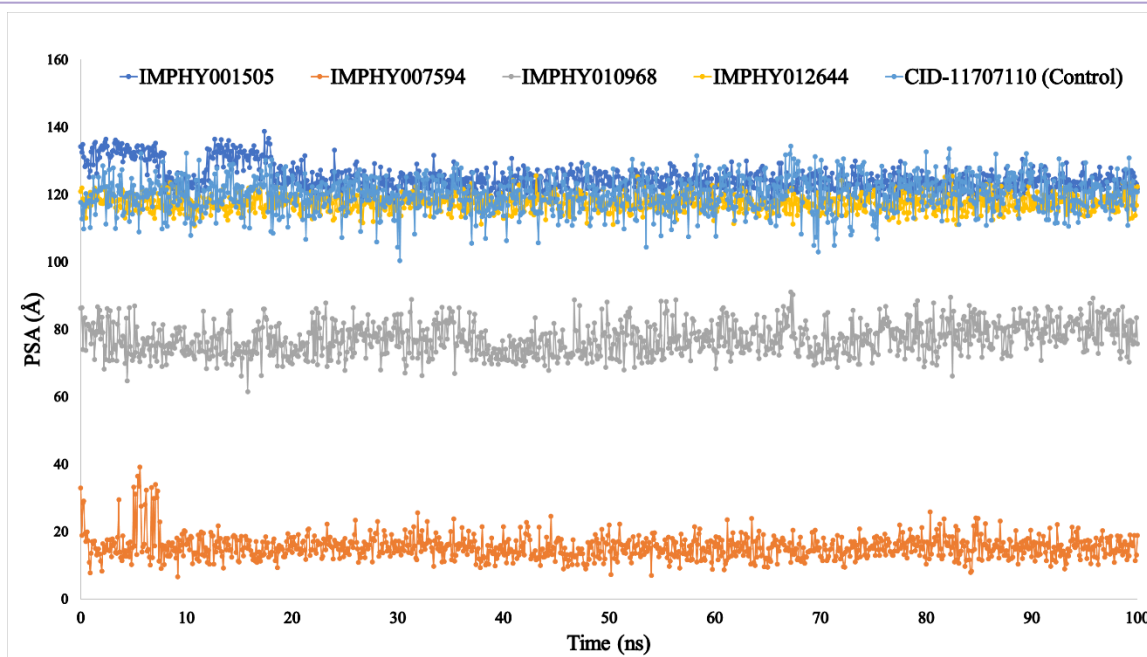


Figure 6: Using a 100 ns simulation interaction diagram (SID), protein-ligand interaction compounds' PSAs were calculated. IMPHY001505, IMPHY010968, IMPHY012644, and the control medication were deep blue, ash, yellow, and blue

Analysis of Intramolecular Bonds

To investigate the intricate arrangement of a protein and its intermolecular interactions with certain ligands, we ran a simulation lasting one hundred nanoseconds (ns) and made use of a tool called the SID.

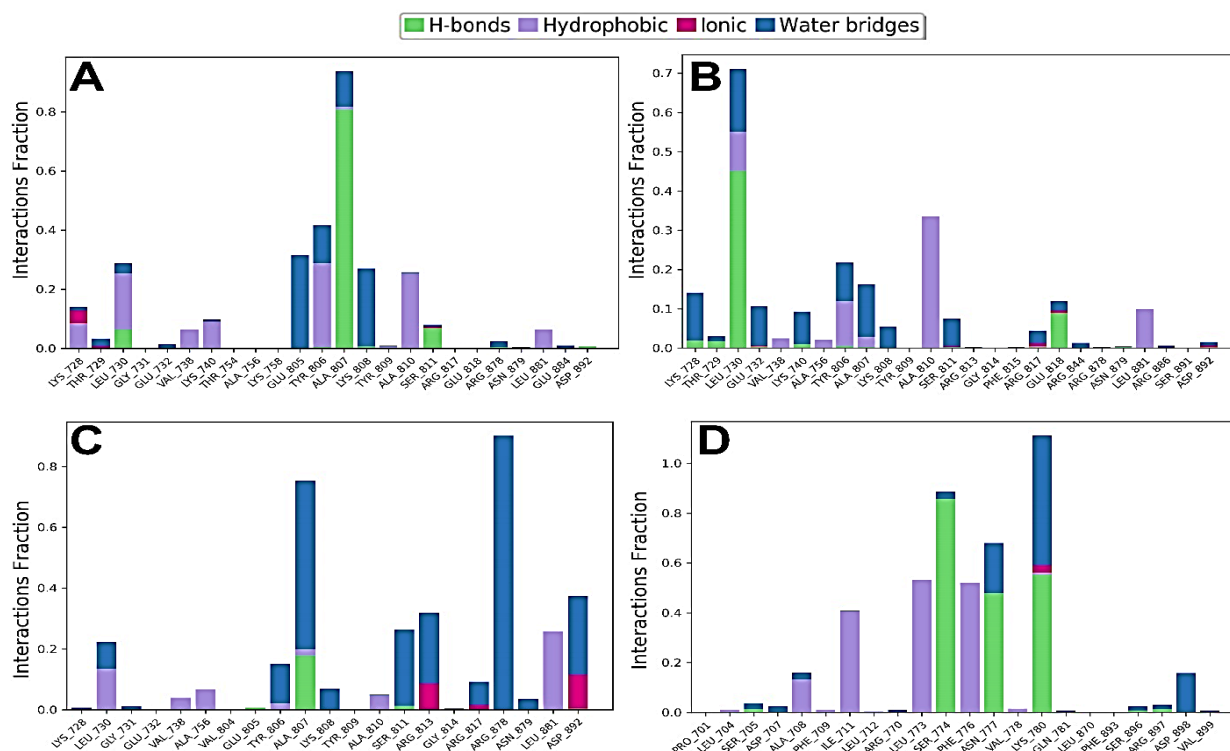


Figure 7: Bar charts showing the interactions between proteins and ligands that were observed during the 100 ns simulation. Specifically, the interactions of four compounds (IMPHY001505, IMPHY010968, IMPHY012644, and a control drug) with the protein are illustrated in this figure. A, B, C, and D correspond to these compounds. The colors used to convey meaning: green represents hydrogen bonds, ash represents hydrophobic bonds, pink is for ionic bonds, and blue is for water bridges.

Figure 7A illustrates the bonds between IMPHY001505 and 6NE7 protein. These bonds consist of hydrogen bonds in the range of 0 to 0.8 interaction fraction, hydrophobic bonds with minimal interaction fraction, and water bridges in the range of 0.8 to 1 interaction fraction.

Figure 7B depicts the bonds between IMPHY010968 and 6NE7 protein, which are composed of hydrogen bonds in the range of 0 to 0.45 interactions fraction, hydrophobic bonds in the range of 0.45 to 0.55 interactions fraction, and water bridges between 0.55 to 7 interactions fraction.

Figure 7C outlines the connections between IMPHY012644 and 6NE7 protein, including hydrogen bonds from 0 to 0.2 interaction fraction, hydrophobic bonds with minimal interaction fractions, and water bridges with a range from 0.2 to 0.75 interaction fractions as well as water bridges with ARG_878 within a range from 00 to 1 interaction fractions.

Lastly, **Figure 7D** illustrates the bonds between the control drug and the 6NE7 protein. The control drug creates Hydrogen bonds with SER_774 within a range of 0 to 0.86 interactions fraction and minimal hydrophobic interactions. Additionally, Hydrogen bonds have been formed between LYS_730 in a fraction range of 0 to 0.56 while also creating minimal hydrophobic interactions and water bridges from 0.58 up to above 1 interaction fraction range.

The comprehensive analysis demonstrates the distinct bonding patterns of the phytochemicals along with the control drug with the target protein, highlighting the intermolecular interactions critical for its binding. Overall, these findings collectively support the observation that IMPHY010968, IMPHY012644, and IMPHY001505 remain in their initial docking positions on RET PROTEIN TYROSINE Kinase, and this stability can be attributed to the specific intermolecular hydrogen bonding patterns elucidated in the figures.

PASS Online Prediction for QSAR Analysis

Using the PASS online tool, three phytochemicals and a control drug were evaluated for their potential to inhibit the tyrosine kinase domain of the RET protein (**Table 6**). Compounds with a higher Pa value are known to have greater pharmacological potency and experimental production potential (Samad et al., 2022). To analyze the quantitative structure-activity relationships (QSAR) of these three phytochemicals and control drugs, we used a Pa cut-off value ≥ 100 (greater than or equal to 100; see **Table 1**). Additionally, PASS can help reduce a molecule's side effects even though it cannot predict binding affinity for new therapeutic targets. After completing an ADME evaluation, the filtered phytochemicals were subjected to site-specific molecular docking analysis.

Table 6: The outcomes of QSAR models for predicting bioactivity in ligand validation

CID	Compounds name	Pa	Pi	Activity
IMPHY001505	Coclaurine	0.008	0.005	Antidyskinetic
		0.730	0.005	MAP kinase stimulant
		0.692	0.018	JAK2 expression inhibitor
		0.644	0.034	Glutamate-5-semialdehyde dehydrogenase inhibitor
		0.676	0.071	Gluconate 2-dehydrogenase (acceptor) inhibitor
		0.618	0.029	Aldehyde oxidase inhibitor
		0.656	0.078	Aspulvinone dimethylallyltransferase inhibitor
		0.573	0.005	NOS2 expression inhibitor
		0.579	0.015	Steroid N-acetylglucosaminyltransferase inhibitor
		0.611	0.059	Chlordecone reductase inhibitor
		0.543	0.004	Tyrosine 3 hydroxylase inhibitor
IMPHY010968	(4S)-10,11-dimethoxyspiro[5-azatricyclo[6.3.1.0 ⁴ ,12] dodeca-1(12),8,10-triene-2,4'-cyclohexa-2,5-diene]-1'-one	0.713	0.049	Gluconate 2-dehydrogenase (acceptor) inhibitor
		0.501	0.050	Aldehyde oxidase inhibitor
		0.409	0.040	Leukopoiesis inhibitor
		0.434	0.073	JAK2 expression inhibitor
		0.392	0.046	CYP2D2 inhibitor
		0.372	0.046	RELA expression inhibitor
		0.331	0.037	Tyrosine 3 hydroxylase inhibitor

		0.385	0.095	Pin1 inhibitor
		0.339	0.063	Steroid N-acetylglucosaminyltransferase inhibitor
		0.308	0.042	NOS2 expression inhibitor
		0.429	0.168	Testosterone 17beta-dehydrogenase (NADP+) inhibitor
IMPHY012644	(-)-Coreximine	0.900	0.200	Antidyskinetic
		0.720	0.015	JAK2 expression inhibitor
		0.749	0.048	Aspulvinone dimethylallyltransferase inhibitor
		0.707	0.007	General pump inhibitor
		0.714	0.049	Gluconate 2-dehydrogenase (acceptor) inhibitor
		0.664	0.004	CYP2D2 inhibitor
		0.620	0.016	Aryl-acylamidase inhibitor
		0.653	0.050	Chlordecone reductase inhibitor
		0.582	0.015	Steroid N-acetylglucosaminyltransferase inhibitor
		0.489	0.010	Monoamine uptake inhibitor
		0.558	0.027	Platelet adhesion inhibitor
		0.524	0.014	Lipid peroxidase inhibitor
		0.544	0.043	Aldehyde oxidase inhibitor
11707110 (control drug)	Trametinib	0.366	0.003	MAP kinase kinase 1 inhibitor
		0.342	0.053	Signal transduction pathways inhibitor
		0.232	0.018	Complement inhibitor
		0.244	0.054	Protein kinase inhibitor
		0.205	0.033	Protein-serine-threonine kinase inhibitor

Analyzing MM-GBSA Results from Post-Molecular Dynamic Simulation Trajectory

The current investigation employed MM/GBSA methodologies to assess the ligand-binding free energy of the designated protein. The analysis of the protein-ligand complex's structure was conducted through the utilization of molecular mechanics/generalized Born surface area (MM/GBSA) calculations. A specific subset of snapshots, each lasting approximately 100 nanoseconds, was chosen from a dynamic simulation trajectory for this analysis.

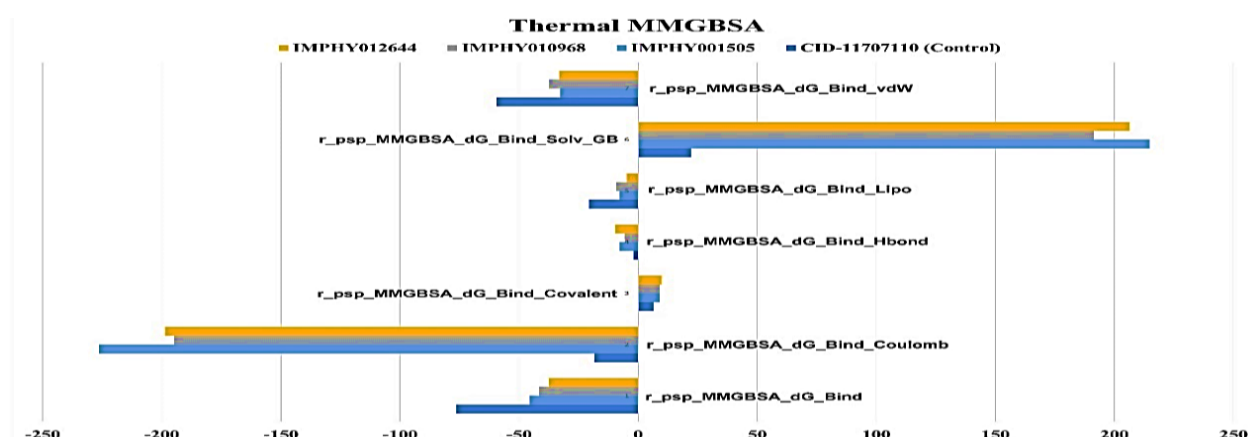


Figure 8: Extracted Snapshots of 6NE7 Protein in the presence of selected compounds: Energy contributions and Net MM/GBSA Binding Free Energy (kcal/mol) with Standard Deviation Values

The evaluation of the complicated shape discovered higher net negative binding unfastened power values of approximately -48kcal/mol, -46 kcal/mol, and -40 kcal/mol for the chosen 3 compounds IMPHY012644, IMPHY010968, and IMPHY001505, respectively, with the centered protein (**Figure 8**). Therefore, it could be considered that the selected compounds might be able to keep a protracted-term interplay with the preferred 6NE7 protein. Our proposed compounds

showed standard values in all calculated parameters compared to the control drug.

Quantum Mechanics Calculation

When determining potential active conformations, binding affinities, and strain factors involved in the binding process, it is crucial to investigate the conformation of a ligand within the protein's binding site. Calculating minimal energy conformations and performing structural optimizations are necessary steps to successfully achieve this type of binding. These steps are dependent on the energies present in the solution phase as well as those related to the gas phase. When it comes to effectively describing ligand-protein complex systems that include metal ions, the traditional molecular mechanics (MM) technique has its drawbacks.

Table 7: Quantum mechanics and HOMO, LUMO analysis of the selected ligands/

Compounds Name	eHOMO (a.u)	eLUMO (a.u)	Gap (a.u)	H (Hardness, Gap/2)	S (Softness, 1/Hardness)
IMPHY001505	-0.19536	-0.00055	0.194811	0.0974055	10.26636073
IMPHY010968	-0.22231	-0.05171	0.170598	0.085299	11.72346686
IMPHY012644	-0.19885	0.004168	0.203018	0.101509	9.851343231
CID-11707110 (control)	-0.20101	-0.05385	0.147164	0.073582	13.59028023

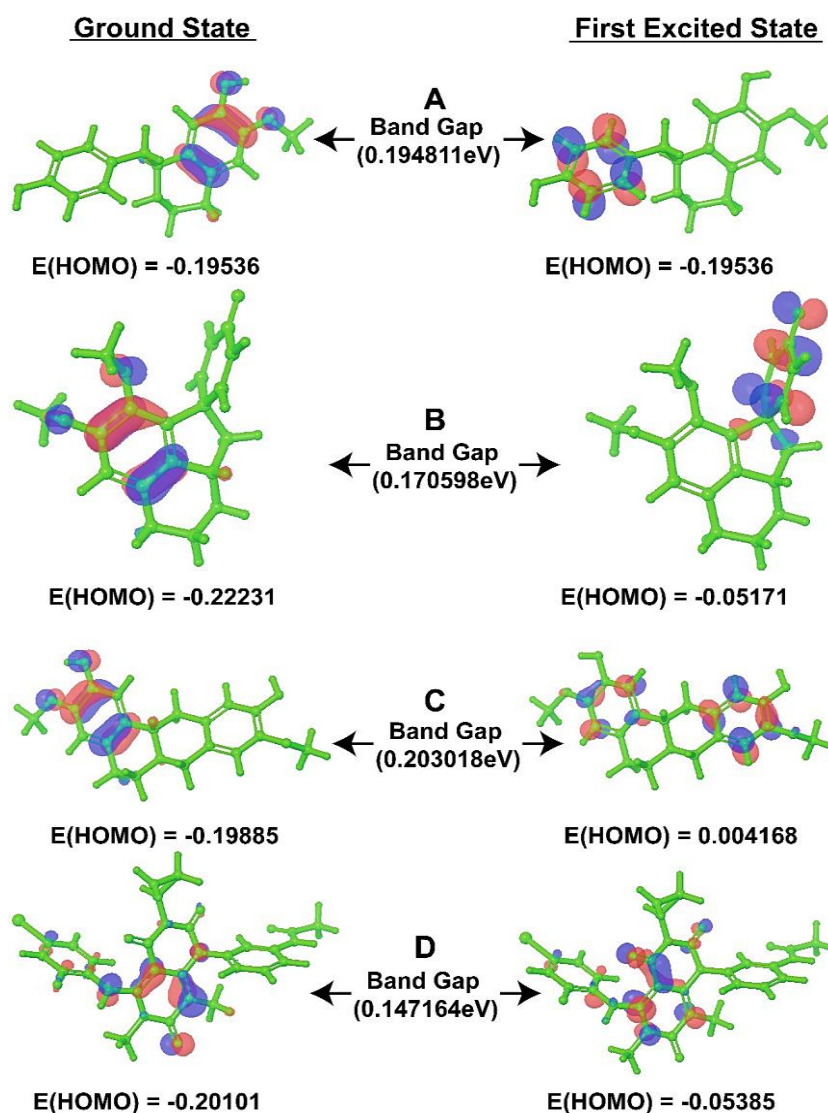


Figure 9: HOMO and LUMO energy scores and structures of the four docked compounds

In the DFT calculations, IMPHY001505 (A), IMPHY010968 (B), IMPHY012644 (C), and CID-11707110 (control) (D)

generated a HOMO energy score of -0.19536 a.u., -0.22231 a.u., -0.19885 a.u., and -0.20101 a.u respectively and LUMO energy score of -0.00055 a.u., -0.05171 a.u., 0.004168 a.u and -0.05385 a.u respectively (**Figure 9**).

IMPHY001505, IMPHY010968, IMPHY012644, and CID-11707110 (control) generated hardness energy of 0.0974055 eV, 0.085299 eV, 0.101509 eV, and 0.073582 eV respectively and softness energy of 10.26636073eV, 11.72346686eV, 9.851343231 eV and 13.59028023 eV respectively (**Table 7**). IMPHY001505, IMPHY010968, and IMPHY012644 compounds were selected and compared with CID-11707110 (control) compounds for more investigation.

4. DISCUSSION

Carcinoma represents the primary cause of global mortality. The incidence of thyroid carcinoma has experienced a notable increase in recent times. Therefore, the examination of mutations in the RET gene carries considerable significance. The identification of mutations in the RET-activating factor has been linked to the causation of C-cell transformation, leading to the subsequent development of Sporadic Medullary Thyroid Cancer (sMTC). Additional research is necessary to ascertain new compounds that can inhibit the RET protein-tyrosine kinase (TK) enzyme (Prescott and Zeiger, 2015). The current investigation employed a comprehensive computational analysis to identify potential pharmaceutical compounds that could selectively target the RET protein, to develop therapeutic interventions for human thyroid carcinoma. The major objective of this research study is to develop effective bioactive compounds that can suppress the overexpression of RET protein. Because by inhibition of overexpression of RET protein, the progression of thyroid carcinoma can be regulated which can be a potential therapeutic option for thyroid cancer.

CADD encompasses diverse, sophisticated functionalities and methodologies, making it a notable instrument for identifying novel compounds targeting specific proteins (Madhavi Sastry et al., 2013). The objective of the CADD approach is to decrease the financial costs and time constraints associated with the overall drug development process. The virtual screening process is specifically designed to integrate a range of computational techniques, such as molecular docking, MM-GBSA, quantum mechanics, MD simulation, ADMET, and other pertinent methodologies. Pharmaceutical research and development heavily rely on the incorporation of this particular component (Bharadwaj et al., 2021).

The goal of this research work was to determine the existence and attributes of the RET protein and to evaluate the effectiveness of different drug candidates using molecular docking and other experimental techniques. The initial stage involved employing a molecular docking methodology to assess the compounds. Subsequently, three phytocompounds were chosen based on their superior negative binding affinity compared to the control ligand, Trametinib. The chosen phytochemicals exhibit lower docking scores compared to Trametinib, which is presently employed as a therapeutic agent for treating thyroid cancer in human patients (Liu et al., 2020)(Zhang et al., 2017).

In the context of the MM-GBSA assay, the optimal ΔG binding score is determined by selecting the value with the most negative score, indicating the lowest score. The MM-GBSA analysis revealed that the three selected compounds and the control compound displayed higher net negative binding free energy values upon binding to the RET protein. As a result, the bond that was not considered was excluded, and the three selected bonds, specifically IMPHY012644, IMPHY010968, IMPHY001505, along with CID-11707110 (as the control), were included for further evaluation using DFT-based computation.

The HOMO-LUMO gap energy is a frequently used term to describe the energy disparity between the HOMO and LUMO. The aforementioned energy denotes the quantity of energy necessary for the excitation of electrons. Compounds that possess a higher orbital gap energy are commonly associated with a more pronounced energetic discrepancy, which consequently makes them less conducive to promoting a chemical reaction. These compounds may be classified as bioactive (Hoque et al., 2015)(Zhan et al., 2003).

The gap energy also affects molecular softness and hardness [76]. The best three ligand compounds were compared to Trametinib using DFT. Finalized ADMET compounds were IMPHY012644, IMPHY010968, IMPHY001505 and CID-11707110 (control).

The finalized three phytochemicals IMPHY012644, IMPHY010968, and IMPHY001505 with control drug Trametinib (CID-11707110) were identified to obey the five criteria of Lipinski's drug-likeness. The phytochemicals with promising ADME properties have been then estimated through the toxicity characteristics to determine the detrimental result on animals or humans (Lipinski, 2004) Investigation of toxicity study established lower toxicity of the selected three phytocompounds (IMPHY012644, IMPHY010968, IMPHY001505) along with Trametinib.

MDS is utilized here to check up the protein-ligand complex stability (Pollastri, 2010)(Aljahdali et al., 2021). It can also identify the rigidity and stability of protein–ligand complexes in distinctly created surroundings like the human body. The

best stability and compactness of the protein-ligand complex is identified by RMSD and RMSF value respectively (Krupanidhi et al., 2021). Our proposed compounds showed promising RMSD and RMSF values. The mass center of the protein N and C terminals examines the protein complex stability and provides a good realization of the characteristics of protein folding (Baidya et al., 2021). Lower radius of gyration value indicates higher compactness and on the other hand, higher radius of gyration value indicates lower compactness. Our selected compounds showed lower Rg values than that of the control drug. Larger SASA values mean more unstable structures. Our selected compounds showed lower Rg values than that of the control drug (Mahmud et al., 2021). Moreover, after the estimation of hydrogen bond interaction, SASA values, MOLSA and PSA values, protein–ligand contact provide promising results for our selected compounds, therefore these phytocompounds are finalized for *in-vitro* and *in-vivo* analysis.

5. CONCLUSION

Three phytochemicals were discovered, and virtual-mediated ADMET screening predicted the best drug-like compounds. Moreover, ADMET (absorption, distribution, metabolism, excretion, and toxicity) analysis, molecular docking, and molecular dynamics simulation successfully induced appropriate bioactive phytocompounds to target the RET protein. The ADMET study revealed their efficacy as potential drug candidates in addition to having no cellular toxicity. The selected bioactive phytocompounds exhibit the highest binding affinity and strong interactions with RET protein catalytic residues. Non-covalent interactions such as hydrophobic interactions and hydrogen bonding were also observed in these protein-ligand complexes. Molecular dynamics simulation proposed that protein-ligand complexes are stable in an artificially created environment and interact most often with RET protein via hydrogen bonds. The investigations found that certain ligand compounds, like Trametinib can suppress carcinoma cell proliferation the most. Drug-like substances interacted with target protein active site residues over long periods. All experiments show that selected drugs interact well with the target receptor, with outstanding values. However, it is essential to acknowledge the limitations inherent in this study. Translating these findings to clinical settings poses challenges, as the simulated environment may not fully capture the complexities of *in vivo* conditions. After the *in vivo* and *in vitro* experiments, it may be possible that the majority of selected bioactive phytocompounds may be used as a possible candidate for RET protein targets of thyroid cancer treatment. Furthermore, the futility limits and safety concerns including dose, side effects, and drug-drug combinations will limit the usage of future anticancer therapies.

Conflict of Interest: The authors declare no conflict of interest.

Author contributions: Conceptualization was carried out by TR, AA, and IAI; TR, AA, AM and KAF developed the methodology; investigation, data curation: TR, AA, AIZ, and MBA; manuscript writing were carried out by TR, AA, MEKT, AM, and AIZ; visualization was carried out by TR, AA, AM, AIZ, IAI, and MTH. AA, IAI, and MEKT reviewed and edited the manuscript; AA, and IAI supervised the project; All authors read and agreed to the published version of the manuscript.

Funding: No funding.

Acknowledgment: The authors acknowledge the International Science Programme (ISP) of Uppsala University in Sweden for financial support.

REFERENCES

- [1] Abdullah, A., Biswas, P., Sahabuddin, M., Mubasharah, A., Khan, D.A., Hossain, A., Roy, T., Rafi, N.M.R., Dey, D., Hasan, M.N., 2023. Molecular Dynamics Simulation and Pharmacoinformatic Integrated Analysis of Bioactive Phytochemicals from *Azadirachta indica* (Neem) to Treat Diabetes Mellitus. *Journal of Chemistry* 2023.
- [2] Ahammad, F., Alam, R., Mahmud, R., Akhter, S., Talukder, E.K., Tonmoy, A.M., Fahim, S., Al-Ghamdi, K., Samad, A., Qadri, I., 2021. Pharmacoinformatics and molecular dynamics simulation-based phytochemical screening of neem plant (*Azadirachta indica*) against human cancer by targeting MCM7 protein. *Briefings in Bioinformatics* 22, bbab098.
- [3] Airaksinen, M.S., Saarna, M., 2002. The GDNF family: Signalling, biological functions and therapeutic value. *Nature Reviews Neuroscience* 3, 383–394.
- [4] Al Saber, Md., Biswas, P., Dey, D., Kaium, Md.A., Islam, Md.A., Tripty, M.I., Rahman, M.D.H., Rahaman, T.I., Biswas, Md.Y., Paul, P., Rahman, Md.A., Hasan, Md.N., Kim, B., 2022. A Comprehensive Review of Recent Advancements in Cancer Immunotherapy and Generation of CAR T Cell by CRISPR-Cas9. *Processes*.
- [5] Aljahdali, M.O., Molla, M.H., Ahammad, F., 2021. Compounds Identified from Marine Mangrove Plant (*Avicennia alba*) as Potential Antiviral Drug Candidates against WDSV, an In-Silico Approach. *Marine Drugs*.
- [6] Arefin, A., Ismail Ema, T., Islam, Tamnia, Hossen, S., Islam, Tariqul, Al Azad, S., Uddin Badal, N., Islam, A., Biswas, P., Alam, N.U., Islam, E., Anjum, M., Masud, A., Kamran, S., Rahman, A., Kumar Paul, P., 2021. Target specificity of selective bioactive compounds in blocking α -dystroglycan receptor to suppress Lassa virus

- infection: an in silico approach. *Journal of biomedical research* 35, 459–473.
- [7] Atofarati, E.O., n.d. MOLECULAR DYNAMICS SIMULATION RESEARCH (FROM ATOMIC FRAGMENTS TO MOLECULAR COMPOUND).
- [8] Baildya, N., Khan, A.A., Ghosh, N.N., Dutta, T., Chattopadhyay, A.P., 2021. Screening of potential drug from *Azadirachta Indica* (Neem) extracts for SARS-CoV-2: An insight from molecular docking and MD-simulation studies. *Journal of Molecular Structure* 1227, 129390.
- [9] Ban, T., Ohue, M., Akiyama, Y., 2018. Multiple grid arrangement improves ligand docking with unknown binding sites: Application to the inverse docking problem. *Computational Biology and Chemistry* 73, 139–146.
- [10] Banegas-Luna, A.-J., Ceron-Carrasco, J.P., Perez-Sanchez, H., 2018. A review of ligand-based virtual screening web tools and screening algorithms in large molecular databases in the age of big data. *Future medicinal chemistry* 10, 2641–2658.
- [11] Baral, S.K., Biswas, P., Kaium, M.A., Islam, M.A., Dey, D., Saber, M. Al, Rahaman, T.I., Emran, T. Bin, Hasan, M.N., Jeong, M.-K., 2022. A comprehensive discussion in vaginal cancer based on mechanisms, treatments, risk factors and prevention. *Frontiers in Oncology* 12, 883805.
- [12] Bharadwaj, S., Dubey, A., Yadava, U., Mishra, S.K., Kang, S.G., Dwivedi, V.D., 2021. Exploration of natural compounds with anti-SARS-CoV-2 activity via inhibition of SARS-CoV-2 Mpro. *Briefings in Bioinformatics* 22, 1361–1377.
- [13] Bhole, R.P., Bonde, C.G., Bonde, S.C., Chikhale, R. V, Wavhale, R.D., 2021. Pharmacophore model and atom-based 3D quantitative structure activity relationship (QSAR) of human immunodeficiency virus-1 (HIV-1) capsid assembly inhibitors. *Journal of Biomolecular Structure and Dynamics* 39, 718–727.
- [14] Bibi, S., Hasan, M.M., Biswas, P., Shkodina, A., Shah, M.A., Shah, G.M., Khan, A., Al-Harrasi, A., 2022. Phytonutrients in the management of lipids metabolism. In: *The Role of Phytonutrients in Metabolic Disorders*. Elsevier, pp. 195–236.
- [15] Biswas, P., Dey, D., Biswas, P.K., Rahaman, T.I., Saha, S., Parvez, A., Khan, D.A., Lily, N.J., Saha, K., Soheli, M., Hasan, M.M., Al Azad, S., Bibi, S., Hasan, Md.N., Rahmatullah, M., Chun, J., Rahman, Md.A., Kim, B., 2022. A Comprehensive Analysis and Anti-Cancer Activities of Quercetin in ROS-Mediated Cancer and Cancer Stem Cells. *International Journal of Molecular Sciences*.
- [16] Biswas, P., Hasan, M.M., Dey, D., dos Santos Costa, A.C., Polash, S.A., Bibi, S., Ferdous, N., Kaium, Md.A., Rahman, M.D.H., Jeet, F.K., Papadakos, S., Islam, K., Uddin, Md.S., 2021. Candidate antiviral drugs for COVID-19 and their environmental implications: a comprehensive analysis. *Environmental Science and Pollution Research* 28, 59570–59593.
- [17] Briggs, P., Winn, M.D., Bailey, S., Ashton, A., 2002. Ccp4 Newsletter on Protein Crystallography. Ccp4.Ac.Uk.Cao, Y., Romero, J., Olson, J.P., Degroote, M., Johnson, P.D., Kieferová, M., Kivlichan, I.D., Menke, T., Peropadre, B., Sawaya, N.P.D., Sim, S., Veis, L., Aspuru-Guzik, A., 2019. Quantum Chemistry in the Age of Quantum Computing. *Chemical Reviews* 119, 10856–10915.
- [18] Ceccherini, I., Boccardi, R., Luo, Y., Pasini, B., Hofstra, R., Takahashi, M., Romeo, G., 1993. Exon Structure and Flanking Intronic Sequences of the Human RET Proto-oncogene. *Biochemical and Biophysical Research Communications* 196, 1288–1295.
- [19] Chagas, C.M., Moss, S., Alisaraie, L., 2018. Drug metabolites and their effects on the development of adverse reactions: Revisiting Lipinski's Rule of Five. *International Journal of Pharmaceutics* 549, 133–149.
- [20] Chen, X., Li, H., Tian, L., Li, Q., Luo, J., Zhang, Y., 2020. Analysis of the Physicochemical Properties of Acaricides Based on Lipinski's Rule of Five. *Journal of Computational Biology* 27, 1397–1406.
- [21] Dallakyan, S., Olson, A.J., 2015. Small-molecule library screening by docking with PyRx. *Methods in Molecular Biology* 1263, 243–250.
- [22] Dey, D., Hossain, R., Biswas, P., Paul, P., Islam, M.A., Ema, T.I., Gain, B.K., Hasan, M.M., Bibi, S., Islam, M.T., 2023. Amentoflavone derivatives significantly act towards the main protease (3CLPRO/MPRO) of SARS-CoV-2: in silico admet profiling, molecular docking, molecular dynamics simulation, network pharmacology. *Molecular diversity* 27, 857–871.
- [23] Dipta, D., Tanzila Ismail, E., Partha Biswas, S.A., Shoeiba Islam, U.R.R., Firoz, M., Ahmed, S.Z., Salauddin, A.L., Rahman, A., Afrin, S., Mahedi, R.A., 2021. Antiviral effects of bacteriocin against animal-to-human transmittable mutated SARS-COV-2: a systematic review. *Front Agric Sci Eng* 8, 603–622.
- [24] Dror, R.O., Arlow, D.H., Maragakis, P., Mildorf, T.J., Pan, A.C., Xu, H., Borhani, D.W., Shaw, D.E., 2011. Activation mechanism of the β 2-adrenergic receptor. *Proceedings of the National Academy of Sciences* 108, 18684–18689.
- [25] Durrant, J.D., Mccammon, J.A., 2011. MD and Drug Design.
- [26] Durrant, J.D., Mccammon, J.A., 2011. Molecular dynamics simulations and drug discovery. *BMC Biology* 9, 71.
- [27] Feng, X.-Y., Jia, W.-Q., Liu, X., Jing, Z., Liu, Y.-Y., Xu, W.-R., Cheng, X.-C., 2019. Identification of novel PPAR α/γ dual agonists by pharmacophore screening, docking analysis, ADMET prediction and molecular dynamics simulations. *Computational Biology and Chemistry* 78, 178–189.

- [28] Ferreira, L.L.G., Andricopulo, A.D., 2019. ADMET modeling approaches in drug discovery. *Drug Discovery Today* 24, 1157–1165.
- [29] Gautschi, O., Milia, J., Filleron, T., Wolf, J., Carbone, D.P., Owen, D., Camidge, R., Narayanan, V., Doebele, R.C., Besse, B., 2017. Targeting RET in patients with RET-rearranged lung cancers: results from the global, multicenter RET registry. *Journal of Clinical Oncology* 35, 1403.
- [30] Genheden, S., Kuhn, O., Mikulskis, P., Hoffmann, D., Ryde, U., 2012. The Normal-Mode Entropy in the MM/GBSA Method: Effect of System Truncation, Buffer Region, and Dielectric Constant. *Journal of Chemical Information and Modeling* 52, 2079–2088.
- [31] Gkeka, P., Stoltz, G., Barati Farimani, A., Belkacemi, Z., Ceriotti, M., Chodera, J.D., Dinner, A.R., Ferguson, A.L., Maillet, J.B., Minoux, H., Peter, C., Pietrucci, F., Silveira, A., Tkatchenko, A., Trstanova, Z., Wiewiora, R., Lelièvre, T., 2020. Machine Learning Force Fields and Coarse-Grained Variables in Molecular Dynamics: Application to Materials and Biological Systems. *Journal of Chemical Theory and Computation* 16, 4757–4775.
- [32] Glassman, P.M., Muzykantov, V.R., 2019. Pharmacokinetic and pharmacodynamic properties of drug delivery systems. *Journal of Pharmacology and Experimental Therapeutics* 370, 570–580.
- [33] Hasan, A., Biswas, P., Bondhon, T.A., Jannat, K., Paul, T.K., Paul, A.K., Jahan, R., Nissapatorn, V., Mahboob, T., Wilairatana, P., 2022. Can artemisia herba-alba be useful for managing COVID-19 and comorbidities? *Molecules* 27, 492.
- [34] Hoque, M.M., Halim, M.A., Sarwar, M.G., Khan, M.W., 2015. Palladium-catalyzed cyclization of 2-alkynyl-N-ethanoyl anilines to indoles: Synthesis, structural, spectroscopic, and mechanistic study. *Journal of Physical Organic Chemistry* 28, 732–742.
- [35] Hossain, A., Rafi, M.A., Mohd., F.-R.-S., Asif, S., Partha, B., Khalil, S.Md.E., Zernaz, A.S., Ismail, E.T., Nova, R., Arif, K.Md., Rahaman, M.Md.F., Bin, E.T., Peng, L., 2023. Role of T cells in cancer immunotherapy: Opportunities and challenges. *Cancer Pathogenesis and Therapy* 01, 116–126.
- [36] Hsiao, Y., Su, B.-H., Tseng, Y.J., 2021. Current development of integrated web servers for preclinical safety and pharmacokinetics assessments in drug development. *Briefings in Bioinformatics* 22, bbaa160.
- [37] Huang, L., Jiang, S., Shi, Y., 2020. Tyrosine kinase inhibitors for solid tumors in the past 20 years (2001–2020). *Journal of Hematology & Oncology* 13, 143.
- [38] Huang, W., Manglik, A., Venkatakrishnan, A.J., Laeremans, T., Feinberg, E.N., Sanborn, A.L., Kato, H.E., Livingston, K.E., Thorsen, T.S., Kling, R.C., Granier, S., Gmeiner, P., Husbands, S.M., Traynor, J.R., Weis, W.I., Steyaert, J., Dror, R.O., Kobilka, B.K., 2015. Structural insights into μ -opioid receptor activation. *Nature* 524, 315–321.
- [39] Iams, W.T., Lovly, C.M., 2018. Stop fRETting the target: next-generation RET inhibitors have arrived. *Cancer discovery* 8, 797–799.
- [40] Islam, M.A., Zilani, M.N.H., Biswas, P., Khan, D.A., Rahman, M.H., Nahid, R., Nahar, N., Samad, A., Ahammad, F., Hasan, M.N., 2022. Evaluation of in vitro and in silico anti-inflammatory potential of some selected medicinal plants of Bangladesh against cyclooxygenase-II enzyme. *Journal of Ethnopharmacology* 285, 114900.
- [41] Jia, C.-Y., Li, J.-Y., Hao, G.-F., Yang, G.-F., 2020. A drug-likeness toolbox facilitates ADMET study in drug discovery. *Drug Discovery Today* 25, 248–258.
- [42] Kaushik, A.C., Kumar, S., Wei, D.Q., Sahi, S., 2018. Structure based virtual screening studies to identify novel potential compounds for GPR142 and their relative dynamic analysis for study of type 2 diabetes. *Frontiers in chemistry* 6, 23.
- [43] Khan, R.A., Hossain, R., Siyadatpanah, A., Al-Khafaji, K., Khalipha, A.B.R., Dey, D., Asha, U.H., Biswas, P., Saikat, A.S.M., Chenari, H.A., 2021. Diterpenes/diterpenoids and their derivatives as potential bioactive leads against dengue virus: a computational and network pharmacology study. *Molecules* 26, 6821.
- [44] Knowles, P.P., Murray-Rust, J., Kjær, S., Scott, R.P., Hanrahan, S., Santoro, M., Ibáñez, C.F., McDonald, N.Q., 2006. Structure and chemical inhibition of the RET tyrosine kinase domain. *Journal of biological chemistry* 281, 33577–33587.
- [45] Ko, J., Murga, L.F., Wei, Y., Ondrechen, M.J., 2005. Prediction of active sites for protein structures from computed chemical properties. *Bioinformatics* 21, i258–i265.
- [46] Krupanidhi, S., Abraham Peele, K., Venkateswarulu, T.C., Ayyagari, V.S., Nazneen Bobby, M., John Babu, D., Venkata Narayana, A., Aishwarya, G., 2021. Screening of phytochemical compounds of *Tinospora cordifolia* for their inhibitory activity on SARS-CoV-2: an in silico study. *Journal of biomolecular structure & dynamics* 39, 5799–5803.
- [47] Larsen, R., Kronenberg, H., 2011. et ad. Williams textbook of endocrinology 12th edition.
- [48] Lipinski, C.A., 2004. Lead- and drug-like compounds: the rule-of-five revolution. *Drug discovery today. Technologies* 1, 337–341.
- [49] Liu, X., Shen, T., Mooers, B.H.M., Hilberg, F., Wu, J., 2018. Drug resistance profiles of mutations in the RET kinase domain. *British Journal of Pharmacology* 175, 3504–3515.
- [50] Liu, Z., Zhang, R., Sun, Z., Yao, J., Yao, P., Chen, X., Wang, X., Gao, M., Wan, J., Du, Y., Zhao, S., 2020. Identification of hub genes and small-molecule compounds in medulloblastoma by integrated bioinformatic

- analyses. PeerJ 2020.
- [51] Madhavi Sastry, G., Adzhigirey, M., Day, T., Annabhimoju, R., Sherman, W., 2013. Protein and ligand preparation: parameters, protocols, and influence on virtual screening enrichments. *Journal of Computer-Aided Molecular Design* 27, 221–234.
 - [52] Mahato, A.K., Sidorova, Y.A., 2020. RET Receptor Tyrosine Kinase: Role in Neurodegeneration, Obesity, and Cancer. *International Journal of Molecular Sciences*.
 - [53] Mahmud, S., Rahman, E., Nain, Z., Billah, M., Karmakar, S., Mohanto, S.C., Paul, G.K., Amin, A., Acharjee, U.K., Saleh, M.A., 2021. Computational discovery of plant-based inhibitors against human carbonic anhydrase IX and molecular dynamics simulation. *Journal of biomolecular structure & dynamics* 39, 2754–2770.
 - [54] MahmutGür EdaAltınöz, NesrinŞener, ÇiğdemŞahin, MerveŞenturan, İzzetŞener, MuhammetÇavuş, Ergin MuratAltuner, M., 2023. Novel 1,3,4-Thiadiazole Derivatives as Antibiofilm, Antimicrobial, Efflux Pump Inhibiting Agents and Their ADMET Characterizations. *Journal* 10, 99–116.
 - [55] Mani, S., Santoro, M., Fusco, A., Billaud, M., Billaud, M., 2001. <Manie 2001.pdf> 17, 580–589.
 - [56] Maurya, A.K., Mulpuru, V., Mishra, N., 2020. Discovery of novel coumarin analogs against the α -glucosidase protein target of Diabetes mellitus: Pharmacophore-based QSAR, docking, and molecular dynamics simulation studies. *ACS omega* 5, 32234–32249.
 - [57] Mohanraj, K., Karthikeyan, B.S., Vivek-Ananth, R.P., Chand, R.P.B., Aparna, S.R., Mangalapandi, P., Samal, A., 2018. IMPPAT: A curated database of Indian Medicinal Plants, *Phytochemistry And Therapeutics. Scientific Reports* 8, 4329.
 - [58] Morshed, A.K.M.H., Al Azad, S., Mia, M.A.R., Uddin, M.F., Ema, T.I., Yeasin, R.B., Srishti, S.A., Sarker, P., Aurthi, R.Y., Jamil, F., 2022. Oncoinformatic screening of the gene clusters involved in the HER2-positive breast cancer formation along with the in silico pharmacodynamic profiling of selective long-chain omega-3 fatty acids as the metastatic antagonists. *Molecular diversity* 1–22.
 - [59] Munshi, M., Zilani, M.N.H., Islam, M.A., Biswas, P., Das, A., Afroz, F., Hasan, M.N., 2022. Novel compounds from endophytic fungi of *Ceriops decandra* inhibit breast cancer cell growth through estrogen receptor alpha in in-silico study. *Informatics in Medicine Unlocked* 32, 101046.
 - [60] Myers, S.M., Eng, C., Ponder, B.A., Mulligan, L.M., 1995. Characterization of RET proto-oncogene 3' splicing variants and polyadenylation sites: a novel C-terminus for RET. *Oncogene* 11, 2039–2045.
 - [61] Neves, B.J., Braga, R.C., Melo-Filho, C.C., Moreira-Filho, J.T., Muratov, E.N., Andrade, C.H., 2018. QSAR-based virtual screening: advances and applications in drug discovery. *Frontiers in pharmacology* 9, 1275.
 - [62] Olubode, S.O., Bankole, M.O., Akinnusi, P.A., Adanlawo, O.S., Ojubola, K.I., Nwankwo, D.O., Edjebah, O.E., Adebesein, A.O., Ayodele, A.O., 2022. Molecular Modeling Studies of Natural Inhibitors of Androgen Signaling in Prostate Cancer. *Cancer Informatics* 21, 11769351221118556.
 - [63] Omar, A.M., Aljahdali, A.S., Safo, M.K., Mohamed, G.A., Ibrahim, S.R.M., 2023. Docking and Molecular Dynamic Investigations of Phenylspirodrimanones as Cannabinoid Receptor-2 Agonists. *Molecules*.
 - [64] Pearson, R.G., 1986. Absolute electronegativity and hardness correlated with molecular orbital theory. *Proceedings of the National Academy of Sciences of the United States of America* 83, 8440–8441.
 - [65] Pollastri, M.P., 2010. Overview on the Rule of Five. *Current protocols in pharmacology* Chapter 9, Unit 9.12.
 - [66] Prescott, J.D., Zeiger, M.A., 2015. The RET oncogene in papillary thyroid carcinoma. *Cancer* 121, 2137–2146.
 - [67] Prete, A., Borges de Souza, P., Censi, S., Muzza, N.N., Sponziello, M., 2020. Update on fundamental mechanisms of thyroid cancer. *Front Endocrinol (Lausanne)* 11: 102.
 - [68] Rahman, M.S., Zilani, M.N.H., Islam, M.A., Hasan, M.M., Islam, M.M., Yasmin, F., Biswas, P., Hirashima, A., Rahman, M.A., Hasan, M.N., 2021. In vivo neuropharmacological potential of gomphandra tetrandra (wall.) sleumer and in-silico study against β -amyloid precursor protein. *Processes* 9, 1449.
 - [69] Roos, K., Wu, C., Damm, W., Reboul, M., Stevenson, J.M., Lu, C., Dahlgren, M.K., Mondal, S., Chen, W., Wang, L., Abel, R., Friesner, R.A., Harder, E.D., 2019. OPLS3e: Extending Force Field Coverage for Drug-Like Small Molecules. *Journal of Chemical Theory and Computation* 15, 1863–1874.
 - [70] Samad, A., Huq, Md.A., Rahman, Md.S., 2022. Bioinformatics approaches identified dasatinib and bortezomib inhibit the activity of MCM7 protein as a potential treatment against human cancer. *Scientific Reports* 12, 1539.
 - [71] Sarker, Md.T., Saha, S., Biswas, P., Islam, Md.T., Sheikh, M.A., Hasan, Md.N., Islam, N., Rabbe, Md.M.I., Rafi, Md.O., 2022. Identification of blood-based inflammatory biomarkers for the early-stage detection of acute myocardial infarction. *Network Modeling Analysis in Health Informatics and Bioinformatics* 11, 28.
 - [72] Stanzione, F., Giangreco, I., Cole, J.C., 2021. Use of molecular docking computational tools in drug discovery. *Progress in Medicinal Chemistry* 60, 273–343.
 - [73] Subbiah, V., Gainor, J.F., Rahal, R., Brubaker, J.D., Kim, J.L., Maynard, M., Hu, W., Cao, Q., Sheets, M.P., Wilson, D., 2018. Precision targeted therapy with BLU-667 for RET-driven cancers. *Cancer discovery* 8, 836–849.
 - [74] Terzyan, S.S., Shen, T., Liu, X., Huang, Q., Teng, P., Zhou, M., Hilberg, F., Cai, J., Mooers, B.H.M., Wu, J., 2019. Structural basis of resistance of mutant RET protein-tyrosine kinase to its inhibitors nintedanib and vandetanib. *Journal of Biological Chemistry* 294, 10428–10437.

- [75] Vargas-Leal, V., Bruno, R., Derfuss, T., Krumbholz, M., Hohlfeld, R., Meinl, E., 2005. Expression and function of glial cell line-derived neurotrophic factor family ligands and their receptors on human immune cells. *The Journal of Immunology* 175, 2301–2308.
- [76] Wells Jr, S.A., Santoro, M., 2009. Targeting the RET pathway in thyroid cancer. *Clinical Cancer Research* 15, 7119–7123.
- [77] Yamaoka, T., Kusumoto, S., Ando, K., Ohba, M., Ohmori, T., 2018. Receptor tyrosine kinase-targeted cancer therapy. *International journal of molecular sciences* 19, 3491.
- [78] Zhan, C.-G., Nichols, J.A., Dixon, D.A., 2003. Ionization Potential, Electron Affinity, Electronegativity, Hardness, and Electron Excitation Energy: Molecular Properties from Density Functional Theory Orbital Energies. *The Journal of Physical Chemistry A* 107, 4184–4195.
- [79] Zhang, X.F., Huang, F.H., Zhang, G.L., Bai, D.P., de Felici, M., Huang, Y.F., Gurunathan, S., 2017. Novel biomolecule lycopene-reduced graphene oxide-silver nanoparticle enhances apoptotic potential of trichostatin A in human ovarian cancer cells (SKOV3). *International Journal of Nanomedicine* 12, 7551–7575.
- [80] Zhou, P., Yang, X.-L., Wang, X.-G., Hu, B., Zhang, L., Zhang, W., Si, H.-R., Zhu, Y., Li, B., Huang, C.-L., Chen, H.-D., Chen, J., Luo, Y., Guo, H., Jiang, R.-D., Liu, M.-Q., Chen, Y., Shen, X.-R., Wang, X., Zheng, X.-S., Zhao, K., Chen, Q.-J., Deng, F., Liu, L.-L., Yan, B., Zhan, F.-X., Wang, Y.-Y., Xiao, G.-F., Shi, Z.-L., 2020. A pneumonia outbreak associated with a new coronavirus of probable bat origin. *Nature* 579, 270–273.